Nanoscale

PAPER

View Article Online
View Journal | View Issue

Check for updates

Cite this: *Nanoscale*, 2025, **17**, 25877

Patterning of layered semiconductor GeS_2 by laser photooxidation and water immersion

Shohi Tahara,[a] Keiji Ueno,[b] Koki Kamiya,[a] Taiga Sakai[a] and Ryo Nouchi *[a]

Received 18th March 2025,
Accepted 9th October 2025

DOI: 10.1039/d5nr01130b

rsc.li/nanoscale

Common patterning methods, such as lithography and laser ablation, have detrimental effects on electronic device components because of lithographic-resist residues and laser-induced heat. These effects are particularly significant in two-dimensional layered materials owing to their ultimate thinness. In this study, a lithography-free patterning method was developed using a laser power lower than that required for laser ablation. This method is based on laser photooxidation and the subsequent etching of the formed oxide. Laser irradiation of exfoliated flakes of GeS_2—a layered semiconductor—and subsequent immersion in water form etched holes with diameters close to the diffraction limit of the irradiated light. The required laser power was 200 times lower than that required for laser ablation, which could significantly mitigate the heat-induced damage. Furthermore, the use of water as an etchant demonstrated the environmentally friendly nature of this method. The proposed method is applicable to materials whose photooxides are soluble in water, and the patterning accuracy can be improved using short-wavelength light and a highly stable mechanical stage.

1. Introduction

Two-dimensional (2D) materials obtained by the exfoliation of layered materials such as graphite and transition-metal dichalcogenides have attracted considerable attention owing to their unique structural and electronic properties.[1–3] They exhibit atomically thin bodies with atomically smooth surfaces because of their 2D crystal structure, which makes them promising for certain electronic device applications such as sensors,[4] tunnel transistors,[5] and secondary batteries.[6] The fabrication of complicated and miniaturized device structures requires microfabrication of device components, for example, to prevent crosstalk from neighboring devices.[7]

Lithographic techniques such as photo- and electron-beam (EB) lithography are widely used for the microfabrication of 2D materials.[8–11] These techniques facilitate the processing of arbitrary shapes through high-spatial-resolution patterning. However, lithographic techniques generally require large-scale apparatus and multistep processes, leading to a high cost and low throughput. In addition, these techniques require polymer resists such as poly(methyl methacrylate) and poly(phthalaldehyde). Resist residues on device components are known to degrade the physical, electrical, and optical properties of 2D materials[12] and hinder the atomic-resolution observations of 2D crystal lattices.[13,14] These adverse effects caused by surface adsorbates are significant for 2D materials because of their ultrahigh surface-to-volume ratios.

Some techniques do not rely on lithographic processes and are free from the problems caused by resist residues. Such resist-free techniques include direct patterning of active device components using EB-induced cross-linking,[15] microprinting using molds,[16] and laser ablation.[17–22] EB-induced cross-linking can form a desired pattern on the micro- to nanometer scale but is only applicable to limited material classes, such as metal–organic frameworks. Microprinting requires prefabrication of molds using lithographic techniques. In contrast, laser ablation is a material-independent process that facilitates the direct drawing of arbitrary patterns, where the irradiation of intense laser light induces the evaporative removal of atoms/molecules owing to the temperature rise at the irradiated spot.[19,20] However, this technique requires a high laser power, which causes severe heat-induced damage.[23] Such heat problems are significant for 2D materials that possess ultra-small heat capacities owing to their atomically thin bodies.

In this paper, a resist-free patterning method with a low laser power is discussed, which can mitigate problems that are especially significant for 2D materials. Specifically, the proposed method exploits local photooxidation *via* direct laser irradiation and etching of the oxide formed using a solvent. The laser power required for photooxidation is generally lower than that required for ablation, allowing resist-free and low-power laser patterning. In this study, water was selected as the solvent (etchant) to demonstrate the environmentally friendly

[a]*Department of Physics and Electronics, Osaka Metropolitan University, Sakai 599-8570, Japan. E-mail: r-nouchi@omu.ac.jp*
[b]*Department of Chemistry, Saitama University, Saitama 338-8570, Japan*

nature of the method. Among various materials whose oxides are water soluble,[24–30] germanium disulfide (GeS_2) with a layered crystal structure was used as the target material. GeS_2 is a wide-bandgap semiconductor (~3.6 eV)[30,31] with predicted high hole mobility[32] and has been reported to be promising for ultraviolet light sensing,[30,31] sodium-ion batteries,[33] and phase-change memory.[34] Photooxidative patterning of GeS_2 can be performed with a size close to the diffraction limit of the irradiated light. The laser power required for the proposed method was approximately 200 times lower than that required for laser ablation. The resist-free, low-power laser patterning method demonstrated here is applicable to any material whose oxides are solvent soluble and is especially effective for patterning nanomaterials that possess ultrahigh surface-to-volume ratios and small heat capacities.

2. Experiments

Highly doped Si wafers with a 285 nm thick thermal oxide layer were used as substrates after being cut into chips. The substrate surface was cleaned using acetone and 2-propanol in an ultrasonic bath followed by oxygen plasma cleaning (18 W, 10 min; PDC-32G, Harrick Plasma). GeS_2 flakes were mechanically exfoliated from the source crystal synthesized *via* the Bridgman method[35] using adhesive tape and then transferred to the substrate. The substrate was then immersed in acetone for 1 min to remove contaminants such as residues from the adhesive tape. A typical Raman scattering spectrum of the flakes is shown in Fig. 1(a). The spectra were acquired using a Raman microscope (Raman-DM, Nanophoton) with an excitation wavelength of 532 nm, a laser power of 1 mW, a 100× objective lens, and an accumulation time of 90 s. A strong peak at 360 cm^{-1} and weak peaks at 335 and approximately 435 cm^{-1} were detected, which were similar to those previously reported in the literature.[30]

The GeS_2 flakes on the substrate were irradiated with laser light at wavelengths of 532 and 785 nm with laser power ranging from 0.1 to 1 mW. Irradiation was performed using the same Raman microscope with a 100× objective lens. The maximum irradiation time was set as 600 s, above which the drift of the microscope stage was significant. The irradiated samples were then immersed in ultrapure water for 1 min to 24 h to etch the oxides formed at the irradiated points. Surface morphologies were observed using the dynamic force mode of an atomic force microscope (AFM; AFM5200S, Hitachi High-Tech) to confirm that the irradiated spots were successfully etched. All experiments were performed at room temperature (25 °C) in ambient air. This procedure is schematically illustrated in Fig. 1(b).

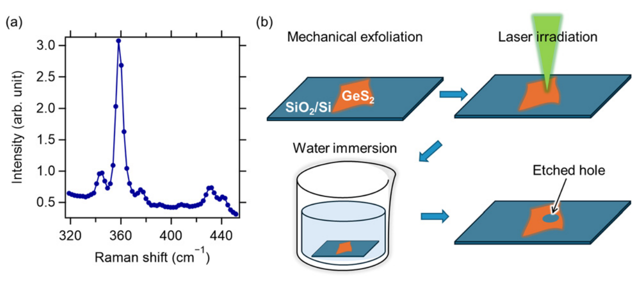

Fig. 1 (a) Raman scattering spectrum of a GeS_2 flake. (b) Schematic of the experimental procedure.

3. Results and discussion

Fig. 2(a–c) show consecutive AFM images of a GeS_2 flake acquired before and after laser irradiation and water immersion, respectively. The two locations indicated in Fig. 2(a) were irradiated with 532 nm laser light with a laser power of 0.96 mW for 80 and 100 s. The substrate was then immersed in water for a certain period and AFM images were acquired again. This process was repeated several times until the total immersion time reached approximately 24 h. As shown in Fig. 2(b), shallow holes formed at the irradiated spots after the first immersion period of 1 min. The depths of the holes further increased with prolonged immersion, as shown in Fig. 2(c). The evolution of the hole depth and flake thickness was plotted against the total immersion time, as shown in Fig. 2(d). The hole depth increased within the first hour but became slightly shallower with further immersion. The flake thickness decreased simultaneously, indicating that the reduction in hole depth was due to a reduction in flake thickness. This slight thinning of the flake could be attributed to the removal of the native oxide layer formed on the surface of GeS_2.[25] These observations led to the conclusion that a sufficient immersion time to accomplish etching was approximately 1 h, which can be further reduced under acidic conditions (see Fig. S1 in the SI). To ensure the complete removal of the formed oxides, an immersion period longer than 20 h was employed in the following experiments, as flake thinning due to the etching of the native oxide layer was limited.

Fig. 3 shows the dependence of the hole depth on the laser power and irradiation time. As shown in Fig. 2, the maximum hole depth was approximately 15 nm, which is smaller than the flake thickness, indicating that the holes did not reach the substrate surface. This could be interpreted as a flake thickness of 32.0 nm, which was too large for the complete photooxidation of the entire thickness. GeS_2 flakes thinner than 15 nm were used to obtain the following results. The thickness of the irradiated spots on the flake, as shown in Fig. 3, was 9.5 or 10.7 nm. Laser irradiation at various powers and periods was conducted along the direction indicated by the arrows in Fig. 3(a). Similar holes are observed after 24 h of immersion in water (Fig. 3(b)). The depth of each hole as determined by AFM is shown in Fig. 3(c). Complete holes reaching the substrate surface were formed by laser irradiation longer than 40 and 70 s at 0.96 and 0.74 mW, respectively. At lower laser powers, a positive correlation between the irradiation time and the hole depth was discernible. Therefore, deeper holes are

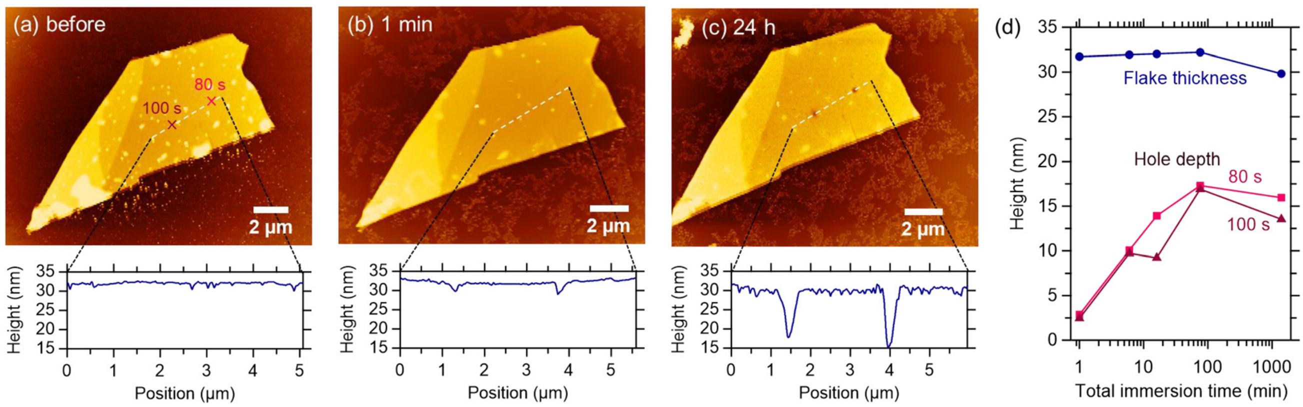

Fig. 2 Dependence on water immersion time, investigated using consecutive AFM images of a GeS_2 flake (a) before 532 nm irradiation, (b) after immersion in water for 1 min, and (c) after immersion in water for approximately 24 h in total. The crosses in (a) indicate the spots irradiated for 80 s and 100 s. The bottom panels show the line profiles along the dashed white lines in the images. The background slopes of the raw data were subtracted by using a linear function. (d) Dependence of the flake thickness and hole depth on immersion time.

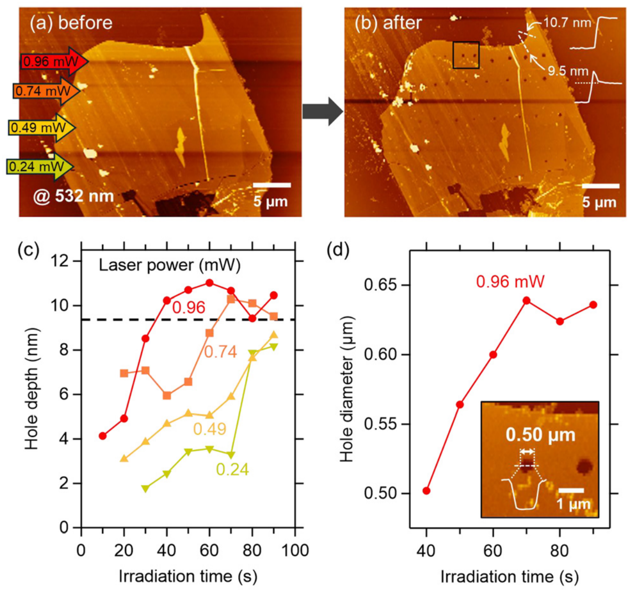

Fig. 3 Dependence of hole depth on irradiation time. AFM images of a GeS_2 flake (a) before 532 nm irradiation and (b) after water immersion. The color and direction of the arrows in (a) represent the laser power used for irradiation and increasing irradiation time, respectively. The insets in (b) show the line profiles at the flake edges. (c) Determined hole depth. The data points above the dashed line were determined to be complete holes that reached the substrate surface. (d) Diameter of complete holes formed by 0.96 mW irradiation. The inset shows a magnified image of the area indicated by the black rectangle in (b). The holes on the left and right sides correspond to 40 and 50 s of irradiation, respectively. The line profile of the left hole is presented in the inset.

expected to be formed by prolonged irradiation, even at lower powers. Fig. 3(d) shows the diameters of the complete holes formed by irradiation at 0.96 mW. The hole diameter increased with the irradiation time, which was ascribed to the fluctuation of the irradiated spot owing to the drift of the sample stage. The smallest diameter was 0.50 µm with a standard deviation of 0.03 µm (see Fig. S2 in the SI), indicating a patterning accuracy close to the diffraction limit of the irradiated light.

Because the data plots in Fig. 3(c) show a positive correlation between the irradiation time and the hole depth, complete holes are expected to be formed by prolonged irradiation, even at lower laser powers. As shown in Fig. 4(a), irradiation

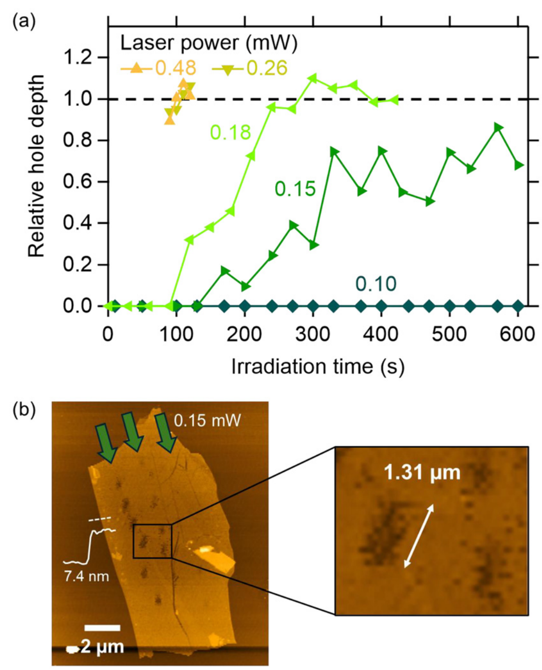

Fig. 4 Effect of prolonged irradiation on hole morphology. (a) Hole depth, normalized to the flake thickness, determined from the AFM images of GeS_2 flakes after water immersion following 532 nm irradiation. The data above the dashed line indicate complete holes reaching the substrate. (b) Representative AFM image of a GeS_2 flake after water immersion and 532 nm irradiation at 0.15 mW. The arrows indicate increasing irradiation time. The line profile at the flake edge is shown. AFM images for other laser powers are provided in Fig. S3 of the SI.

for longer periods resulted in the formation of complete holes with insufficient laser power, as shown in Fig. 3 (see the data for 0.48 and 0.26 mW). Prolonged irradiation for more than 400 s resulted in the formation of a complete hole even at 0.18 mW. However, as shown in Fig. 4(b), the holes formed by prolonged irradiation exhibited an elongated shape, and their lateral dimension reached up to 1.31 µm under irradiation at 0.15 mW. This value exceeds those of holes produced by higher-power irradiation, as shown in Fig. 3, which is attributable to the stage drift. Even when the irradiation time was increased to 600 s, no holes were formed upon irradiation at 0.15 mW. Because the stage drift was significant, irradiation for longer periods was not performed. The shallowest hole formed by irradiation at 0.15 mW exhibited a depth of approximately 1 nm (see Fig. S4 in the SI), demonstrating that the proposed method is capable of generating holes with depths reaching the monolayer level. In addition, irradiation at 0.10 mW resulted in no hole formation (see Fig. S3 in the SI). From the dataset shown in Fig. 4(a), the threshold laser powers for photooxidation and complete hole formation under the present conditions were found to be 0.15 and 0.18 mW, respectively.

To investigate the dependence on the irradiation wavelength, laser irradiation at 785 nm was examined, as shown in Fig. 5. Irradiation was conducted at various laser powers (1.00, 0.73, 0.50, and 0.24 mW) for periods ranging from 10 s to 90 s. Careful examination of the AFM images acquired after water immersion for 24 h (Fig. 5(b)) revealed that no holes were discernible at any of the irradiated spots, regardless of the laser power or irradiation time. The absence of holes after water immersion, despite the flake thickness, laser power, and irradiation time being similar to those used for 532 nm irradiation (Fig. 3), indicated that photooxidation was not induced by 785 nm irradiation.

Generally, the spot diameter is proportional to the wavelength. Consequently, the laser power density (irradiance) was lower for 785 nm irradiation. Specifically, the irradiance at 785 nm was $(532/785)^2$ = 0.46 times that at 532 nm. While 785 nm irradiation at 1.00 mW for 90 s did not induce hole formation (Fig. 5), 532 nm irradiation at nearly the same irradiance (0.49 mW) for 90 s produced an 8 nm-deep hole, as shown in Fig. 3(c). Therefore, the wavelength dependence cannot be attributed to differences in spot size.

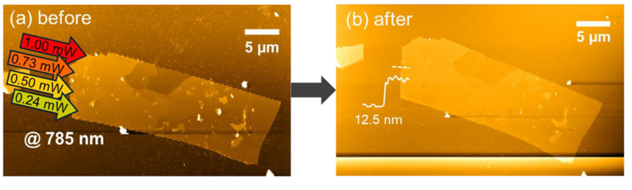

Fig. 5 Inability to induce photooxidation by 785 nm irradiation. AFM images of a GeS_2 flake acquired (a) before 785 nm irradiation and (b) after water immersion. The color and direction of the arrows in (a) represent the laser power used for irradiation and increasing irradiation time, respectively. The inset in (b) shows the line profile at the flake edges.

Photooxidation of GeS_2 requires photoexcitation above the bandgap (E_g = 3.6 eV),[30,31] where Ge–S bonds are cleaved by the above-bandgap excitation and Ge–O bonds are formed instead in the presence of oxygen.[36,37] This requirement has been demonstrated for monolayer WS_2, where oxidation proceeds only under above-bandgap illumination.[38] Furthermore, the presence of environmental water significantly enhances the photooxidation of monolayer WS_2.[39] These findings suggest that both photogenerated electrons and holes contribute to the photooxidation process: electrons reduce adsorbed O_2 molecules to form superoxide anions, while holes oxidize water to generate hydroxyl radicals.[40] These reactive oxygen species, including superoxide and hydroxyl radicals, subsequently oxidize the semiconductor surface. Among the oxidation products, SO_x species are likely to desorb into the air, whereas GeO_x remains within the film and can be removed by immersion in water. In this study, humidity during laser irradiation was not controlled; therefore, the relative contribution of water photolysis on semiconductor surfaces[41–44] remains to be clarified.

Considering the energies of light with wavelengths of 532 and 785 nm, which are 2.33 and 1.58 eV, respectively, excitation with both of these wavelengths does not exceed the E_g of GeS_2. If two-photon absorption[45] is considered, 532 and 785 nm irradiation can possess energies of 4.66 and 3.16 eV, respectively. As shown schematically in Fig. 6(a), only the two-

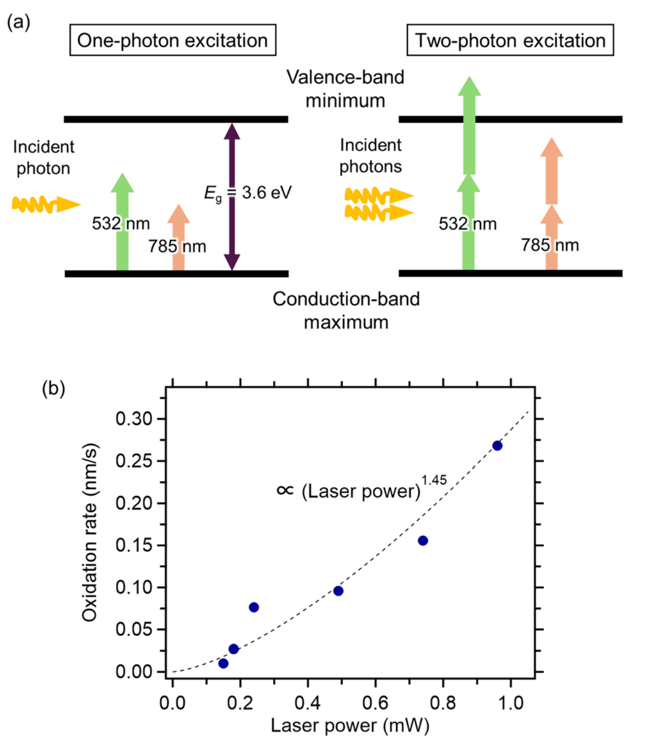

Fig. 6 Photooxidation mechanism *via* two-photon absorption. (a) Overview of one- and two-photon absorption processes. Only two-photon absorption at 532 nm causes excitation above the bandgap of GeS_2. (b) Dependence of the oxidation rate on laser power. The dashed line shows the power-law fit.

photon absorption at 532 nm surpassed E_g. These observations suggest that laser photooxidation of GeS_2 under the present conditions is a two-photon process. To further examine this, we analyzed the laser power dependence data presented in Fig. 3 and 4. First, the photooxidation rate at each laser power was determined by linear fitting of the hole depth as a function of irradiation time (see Fig. S5 in the SI). Next, the calculated rates were plotted against laser power, and the data were fitted to a power function, as shown in Fig. 6(b). The exponent of this function indicates the number of photons involved in the reaction.[46,47] In the present case, the exponent was found to be 1.45, suggesting that more than one photon participates in the process. An exponent less than 2 implies the presence of decay pathways for photoexcited carriers. The photoluminescence spectrum of GeS_2 exhibits a small peak at 1000 nm (see Fig. S6 in the SI), which likely corresponds to defect-related states and promotes rapid recombination of photoexcited carriers before photooxidation occurs. Additionally, the requirement for oxygen diffusion from the top surface may also contribute to the reduction of the exponent from 2.

Finally, the power required for laser ablation was investigated for comparison with the photooxidation-based method. Laser irradiation was performed at a wavelength of 532 nm and various laser powers for different periods. Unlike the photooxidation experiments shown in Fig. 2–5, AFM images were acquired after irradiation without water immersion (Fig. 7(a)). Unlike the photooxidation-based method, there was no positive correlation between the hole depth and the irradiation time (see Fig. S7 in the SI). Deep holes were preferentially formed under short-period irradiation with a high laser power. To investigate the difference between long- and short-period irradiation, laser irradiation with various laser powers at fixed periods of 100 s and 10 s was conducted, as shown in Fig. 7(b) and (c), respectively. In the case of long-period irradiation, the relative hole depths were less than 1 within the investigated range of laser power, indicating that complete holes were not formed. Instead, irradiation at a high power ($\gtrsim$ 30 mW) tended to form large bumps, as shown in the inset of Fig. 7(b). Bump formation can be attributed to repeated melting and agglomeration owing to the heat generated by the high laser power. In contrast, short-period irradiation can form complete holes at laser powers higher than 40 mW. As shown in the inset of Fig. 7(c), the area affected by the laser irradiation was three times larger than the minimum diameter obtained using the photooxidation-based method, which was ascribed to the heat-induced formation of bumps around the holes. As elucidated in the long history of ablation research,[48] a short irradiation time was effective for laser ablation in this case. The threshold laser power for complete hole formation by ablation was determined to be approximately 40 mW for crystalline GeS_2 flakes, which is 200 times higher than that of the photooxidation-based method.

In a previous study on pulsed-laser ablation of amorphous GeS_2,[49] the threshold laser fluence for the formation of craters with depths in the same range as the flake thicknesses used in

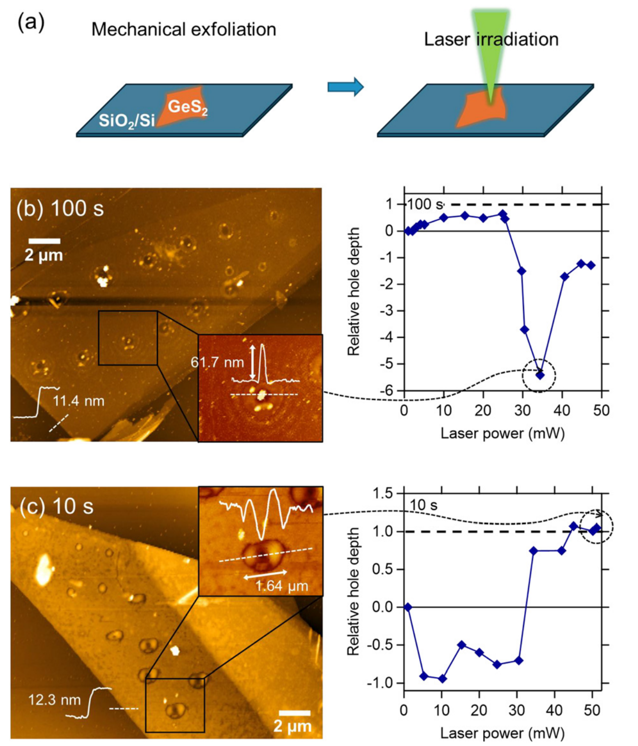

Fig. 7 Dependence of laser power and irradiation time on laser ablation in GeS_2 flakes under 532 nm irradiation. (a) Schematic of the experimental procedure. (b and c) AFM images obtained after fixed irradiation times (left) and the corresponding hole depth as a function of laser power (right), normalized to the flake thickness. The negative depth values indicate bump formation. Irradiation times: (b) 100 s and (c) 10 s. The insets show the line profiles at the flake edges and the magnified images of selected regions.

the present study was found to be approximately 0.05 J cm^{-2}, where holes with a 25 μm diameter were formed by 15 light pulses of 5 ns duration at 213 nm. The threshold laser power could be calculated as $0.05\ \mathrm{J\ cm^{-2}} \times \pi(12.5\ \mu\mathrm{m})^2 \div (15 \times 5\ \mathrm{ns}) = 3.3\ \mathrm{W}$, which was one order of magnitude lower than the threshold power obtained above. This difference in threshold laser power was reasonable considering the crystalline nature of the flakes used in this study.

The primary objective of this study is to develop a novel patterning method specifically tailored for 2D materials. Due to the ultrathin nature of 2D materials, it is essential to mitigate the effects of surface adsorbates and process-induced heat. The proposed method achieves high patterning precision while effectively suppressing these two detrimental effects (see Table S1 in the SI). Several perovskite-type oxides, such as $Sr_3Al_2O_6$,[50] AVO_3 (A = Sr and Ca),[51] and $AMoO_3$ (A = Ca, Sr, and Ba),[52] are known to be water soluble and have been employed as sacrificial layers for the fabrication of free-standing oxide membranes. In addition, metal oxides with high oxidation states, such as MoO_3,[53] CrO_3,[54] and V_2O_5,[55] are generally known to be water soluble. Under weakly acidic or basic conditions, various oxides, such as ZnO,[56,57] CuO,[58] and PbO_2,[59] can also exhibit appreciable water solubility. Therefore, chemical compounds containing these metals are considered possible candidates for the technique discussed in this study.

4. Conclusions

A lithography-free patterning method that can be achieved with a laser power lower than the ablation power was demonstrated based on the laser photooxidation of layered GeS_2 crystals and subsequent etching of oxides by water immersion. This is an environmentally friendly process because water is used as the etchant. The laser power required for the photooxidation of GeS_2 was 200 times lower than that required for laser ablation, which was expected to significantly mitigate the heat-induced damage caused during laser irradiation. In addition, the minimum diameter of the etched holes formed by the proposed method was found to be close to the diffraction limit of the irradiated light (0.50 μm with 532 nm irradiation). Furthermore, the minimum diameter was one-third of the area affected by hole formation due to laser ablation. Because the diameters of the holes were limited by the laser spot size and the drift of the sample stage, the patterning accuracy of the proposed method could be further improved using light with shorter wavelengths and sample stages with higher stability.

Conflicts of interest

There are no conflicts to declare.

Data availability

The data supporting this article have been included as part of the supplementary information (SI). Supplementary information is available. See DOI: https://doi.org/10.1039/d5nr01130b.

Acknowledgements

This study was supported by JSPS KAKENHI Grant Numbers JP22H01912, JP23K23180, and JP22H05445 and JST PRESTO Grant Number JPMJPR20T8.

References

1 V. Shanmugam, R. A. Mensah, K. Babu, S. Gawusu, A. Chanda, Y. Tu, R. E. Neisiany, M. Försth, G. Sas and O. Das, *Part. Part. Syst. Charact.*, 2022, **39**, 2200031.
2 X. Huang, C. Liu and P. Zhou, *npj 2D Mater. Appl.*, 2022, **6**, 1–19.
3 T. Dutta, N. Yadav, Y. Wu, G. J. Cheng, X. Liang, S. Ramakrishna, A. Sbai, R. Gupta, A. Mondal, Z. Hongyu and A. Yadav, *Nano Mater. Sci.*, 2024, **6**, 1–23.
4 M. V. Sulleiro, A. Dominguez-Alfaro, N. Alegret, A. Silvestri and I. J. Gómez, *Sens. Biosensing Res.*, 2022, **38**, 100540.
5 S. Kanungo, G. Ahmad, P. Sahatiya, A. Mukhopadhyay and S. Chattopadhyay, *npj 2D Mater. Appl.*, 2022, **6**, 1–29.
6 Y. He, X. Shen and Y. Zhang, *ACS Appl. Nano Mater.*, 2024, **7**, 27907–27939.
7 M. Li, Q. Tang, Y. Tong, X. Zhao, S. Zhou and Y. Liu, *Appl. Phys. Express*, 2018, **11**, 036502.
8 Z. Gao, H. Kang, C. H. Naylor, F. Streller, P. Ducos, M. D. Serrano, J. Ping, J. Zauberman, Rajesh, R. W. Carpick, Y.-J. Wang, Y. W. Park, Z. Luo, L. Ren and A. T. C. Johnson, *ACS Appl. Mater. Interfaces*, 2016, **8**, 27546–27552.
9 M. Kim, D. Ha and T. Kim, *Nat. Commun.*, 2015, **6**, 6247.
10 H. Park, J. Mun, D. Joung, J. J. Wie, S.-H. Jeong and S.-W. Kang, *Chem. Eng. J.*, 2020, **382**, 122944.
11 G. Yoon, I. Kim, S. So, J. Mun, M. Kim and J. Rho, *Sci. Rep.*, 2017, **7**, 6668.
12 J. Liang, K. Xu, B. Toncini, B. Bersch, B. Jariwala, Y.-C. Lin, J. Robinson and S. K. Fullerton-Shirey, *Adv. Mater. Interfaces*, 2019, **6**, 1801321.
13 M. Ishigami, J. H. Chen, W. G. Cullen, M. S. Fuhrer and E. D. Williams, *Nano Lett.*, 2007, **7**, 1643–1648.
14 M. T. Pettes, I. Jo, Z. Yao and L. Shi, *Nano Lett.*, 2011, **11**, 1195–1200.
15 X. Tian, F. Li, Z. Tang, S. Wang, K. Weng, D. Liu, S. Lu, W. Liu, Z. Fu, W. Li, H. Qiu, M. Tu, H. Zhang and J. Li, *Nat. Commun.*, 2024, **15**, 2920.
16 W. Zheng, T. Xie, Y. Zhou, Y. L. Chen, W. Jiang, S. Zhao, J. Wu, Y. Jing, Y. Wu, G. Chen, Y. Guo, J. Yin, S. Huang, H. Q. Xu, Z. Liu and H. Peng, *Nat. Commun.*, 2015, **6**, 6972.
17 R. Li, L. M. Schneider, W. Heimbrodt, H. Wu, M. Koch and A. Rahimi-Iman, *Sci. Rep.*, 2016, **6**, 28224.
18 D. Shen, X. Zhang and L. Zhu, *Nano Energy*, 2024, **120**, 109182.
19 A. V. Emelianov, M. Pettersson and I. I. Bobrinetskiy, *Adv. Mater.*, 2024, **36**, 2402907.
20 C. Kerse, H. Kalaycıoğlu, P. Elahi, B. Çetin, D. K. Kesim, Ö. Akçaalan, S. Yavaş, M. D. Aşık, B. Öktem, H. Hoogland, R. Holzwarth and F. Ö. Ilday, *Nature*, 2016, **537**, 84–88.
21 D. Shen, X. Zhang and L. Zhu, *Nano Energy*, 2024, **120**, 109182.
22 A. V. Emelianov, M. Pettersson and I. I. Bobrinetskiy, *Adv. Mater.*, 2024, **36**, 2402907.
23 K.-W. Kim, S. J. Park, S.-J. Park, I. Kim, B. Park, S. H. Kim, U. Jeong, J. K. Kim and C. Yang, *npj Flexible Electron.*, 2024, **8**, 1–9.
24 S. H. Jin, S.-K. Kang, I.-T. Cho, S. Y. Han, H. U. Chung, D. J. Lee, J. Shin, G. W. Baek, T. Kim, J.-H. Lee and J. A. Rogers, *ACS Appl. Mater. Interfaces*, 2015, **7**, 8268–8274.
25 J. Sun, G. Giorgi, M. Palummo, P. Sutter, M. Passacantando and L. Camilli, *ACS Nano*, 2020, **14**, 4861–4870.
26 J. G. Connell, B. J. Isaac, G. B. Ekanayake, D. R. Strachan and S. S. A. Seo, *Appl. Phys. Lett.*, 2012, **101**, 251607.
27 T. Harada and A. Tsukazaki, *AIP Adv.*, 2017, **7**, 085011.
28 D. Lu, D. J. Baek, S. S. Hong, L. F. Kourkoutis, Y. Hikita and H. Y. Hwang, *Nat. Mater.*, 2016, **15**, 1255–1260.

29 I. S. Khan, W. E. McMahon, C.-S. Jiang, P. Walker, A. Zakutayev and A. G. Norman, *Cryst. Growth Des.*, 2024, **24**, 7389–7395.
30 Y. Yang, S.-C. Liu, X. Wang, Z. Li, Y. Zhang, G. Zhang, D.-J. Xue and J.-S. Hu, *Adv. Funct. Mater.*, 2019, **29**, 1900411.
31 S. Chen, B. Cao, W. Wang, X. Tang, Y. Zheng, J. Chai, D. Kong, L. Chen, S. Zhang and G. Li, *Appl. Phys. Lett.*, 2022, **120**, 111101.
32 Y. Mao and G. Zhang, *Physica B*, 2020, **581**, 411673.
33 C. C. Li, B. Wang, D. Chen, L.-Y. Gan, Y. Feng, Y. Zhang, Y. Yang, H. Geng, X. Rui and Y. Yu, *ACS Nano*, 2020, **14**, 531–540.
34 X. Wang, J. Tan, C. Han, J.-J. Wang, L. Lu, H. Du, C.-L. Jia, V. L. Deringer, J. Zhou and W. Zhang, *ACS Nano*, 2020, **14**, 4456–4462.
35 A. V. Golubkov, G. B. Dubrovskii and A. I. Shelykh, *Semiconductors*, 1998, **32**, 734–735.
36 J. H. Horton, K. L. Peat and R. M. Lambert, *J. Phys.: Condens. Matter*, 1993, **5**, 9037.
37 A. C. Mendes, L. J. Q. Maia, S. H. Messaddeq, Y. Messaddeq, A. R. Zanatta and M. Siu Li, *Curr. Appl. Phys.*, 2010, **10**, 1411–1415.
38 J. C. Kotsakidis, Q. Zhang, A. L. Vazquez de Parga, M. Currie, K. Helmerson, D. K. Gaskill and M. S. Fuhrer, *Nano Lett.*, 2019, **19**, 5205–5215.
39 P. Atkin, D. W. M. Lau, Q. Zhang, C. Zheng, K. J. Berean, M. R. Field, J. Z. Ou, I. S. Cole, T. Daeneke and K. Kalantar-Zadeh, *2D Mater.*, 2017, **5**, 015013.
40 Y. Nosaka and A. Y. Nosaka, *Chem. Rev.*, 2017, **117**, 11302–11336.
41 B. Giri, M. Masroor, T. Yan, K. Kushnir, A. D. Carl, C. Doiron, H. Zhang, Y. Zhao, A. McClelland, G. A. Tompsett, D. Wang, R. L. Grimm, L. V. Titova and P. M. Rao, *Adv. Energy Mater.*, 2019, **9**, 1901236.
42 J. Lin, Z. Zhang, J. Chai, B. Cao, X. Deng, W. Wang, X. Liu and G. Li, *Small*, 2021, **17**, 2006666.
43 S. Xie, J. Liang, Q. Liu, P. Liu, J. Wang, J. Li, H. Wu, W. Wang and G. Li, *J. Mater. Chem. A*, 2023, **11**, 25671–25682.
44 D. Liu and Y. Kuang, *Adv. Mater.*, 2024, **36**, 2311692.
45 P. T. C. So, C. Y. Dong, B. R. Masters and K. M. Berland, *Annu. Rev. Biomed. Eng.*, 2000, **2**, 399–429.
46 M. B. Masthay, A. E. Beach, R. M. Eckerle, B. Fouzia, P. W. Hovey, D. W. Johnson, R. E. Jones, M. E. Kelleher, P. Limphong, J. B. McGregor, R. J. Provost, T. C. Sack, C. M. Shover, W. Wang, Y. Zhao and M. C. Helvenston, *J. Photochem. Photobiol., A*, 2024, **452**, 115528.
47 Y. Tominari, T. Yamada, T. Kaji, C. Yamada and A. Otomo, *Jpn. J. Appl. Phys.*, 2021, **60**, 101002.
48 R. E. Russo, *Appl. Phys. A*, 2023, **129**, 168.
49 P. Kutálek, P. Knotek, A. Šandová, T. Vaculovič, E. Černošková and L. Tichý, *Appl. Surf. Sci.*, 2021, **554**, 149582.
50 P. Salles, I. Caño, R. Guzman, C. Dore, A. Mihi, W. Zhou and M. Coll, *Adv. Mater. Interfaces*, 2021, **8**, 2001643.
51 V. Polewczyk, B. Bérini, A. Cheikh, D. Dagur, M. Mezhoud, O. El-Khaloufi, M. Mebarki, L. Braglia, S. Hurand, A. Fouchet, G. Vinai, P. Torelli, A. David, Y. Dumont and U. Lüders, *Adv. Mater. Interfaces*, 2025, **12**, 2500094.
52 M. Mebarki, B. Bérini, V. Polewczyk, A. Fouchet, V. Demange and Y. Dumont, *ACS Appl. Mater. Interfaces*, 2025, **17**, 27400–27407.
53 K. Saidov, I. Erofeev, Z. Aabdin, A. Pacco, H. Philipsen, A. W. Hartanto, Y. Chen, H. Yan, W. W. Tjiu, F. Holsteyns and U. Mirsaidov, *Adv. Funct. Mater.*, 2024, **34**, 2310838.
54 S. Kumar, H. Suresh, V. A. Sethuraman, P. Kumar and R. Pratap, *SN Appl. Sci.*, 2020, **2**, 2073.
55 M. Aslam, I. M. I. Ismail, N. Salah, S. Chandrasekaran, M. T. Qamar and A. Hameed, *J. Hazard. Mater.*, 2015, **286**, 127–135.
56 X. Wang, T. Sun, H. Zhu, T. Han, J. Wang and H. Dai, *J. Environ. Manage.*, 2020, **267**, 110656.
57 J. Han, W. Qiu and W. Gao, *J. Hazard. Mater.*, 2010, **178**, 115–122.
58 N. Odzak, D. Kistler, R. Behra and L. Sigg, *Environ. Pollut.*, 2014, **191**, 132–138.
59 Y. Xie, Y. Wang, V. Singhal and D. E. Giammar, *Environ. Sci. Technol.*, 2010, **44**, 1093–1099.